Research Article

Intense violet–blue emission and paramagnetism of nanocrystalline Gd³⁺ doped ZnO ceramics

S. SAMBASIVAM[a,b,*], D. PAUL JOSEPH[c], S. ASIRI NAIDU[d], K. N. HUI[e], K. S. HUI[f], B. C. CHOI[a,*]

[a]*Department of Physics, Pukyong National University, Busan 608-737, Republic of Korea*
[b]*Department of Physics, Velammal Institute of Technology, Chennai 601204, India*
[c]*Department of Physics, National Institute of Technology, Warangal, Telangana 506004, India*
[d]*Rajiv Gandhi University of Knowledge Technologies, Nuzvid, Andhra Pradesh 521201, India*
[e]*Institute of Applied Physics and Materials Engineering, University of Macau, Avenida da Universidade, Taipa, Macau, China*
[f]*Department of Mechanical Convergence Engineering, Hanyang University, 17 Haengdang-dong, Seongdong-gu, Seoul 133-791, Republic of Korea*

Abstract: Nanocrystalline $Zn_{1-x}Gd_xO$ ($x = 0$, 0.02, 0.04, 0.06, and 0.08) ceramics were synthesized by ball milling and subsequent solid-state reaction. The transmission electron microscopy (TEM) micrograph of as synthesized samples revealed the formation of crystallites with an average diameter of 60 nm, and the selected area electron diffraction (SAED) pattern confirmed the formation of wurtzite structure. A red shift in the band gap was observed with increasing Gd^{3+} concentration. The photoluminescence of nanocrystalline Gd^{3+} doped ZnO exhibited a strong violet–blue emission. Concentration dependence of the emission intensity of Gd^{3+} in ZnO was studied, and the critical concentration was found to be 4 mol% of Gd^{3+}. The Gd^{3+} doped ZnO exhibited paramagnetic behavior at room temperature, and the magnetic moment increased with Gd^{3+} concentration.

Keywords: X-ray diffraction (XRD); nano-ceramics; rare earth element; semiconductors

1 Introduction

Zinc oxide is one of the most important semiconductor materials with a direct wide band gap of 3.37 eV and a large exciton binding energy of 60 meV at room temperature which is much larger than that of GaN (25 meV), and is proved to be important for blue/UV optical devices [1]. In addition to larger exciton binding energy, the ability to grow the single crystal substrates makes the material more promising. The new perspectives of ZnO include blue/UV optoelectronics, transparent electronics, spintronics, and sensors [2,3]. In recent years, rare earth (RE) doped oxide semiconductors (e.g., ZnO, SnO₂) have been the focus of numerous investigations because of their short luminescence life time, cathodo-luminescence, electro-luminescence, and possibility to tune the emission properties with crystallite size [4–7]. Rare earth ions are used as activators since their emission can be fine tuned with respect to the host

* Corresponding authors.
E-mail: S. Sambasivam, sambaphy@gmail.com;
          B. C. Choi, bcchoi@pknu.ac.kr

lattice for the full color emission (white light). Ney *et al*. [8] have reported a broad red emission in ZnO single crystals by doping Gd^{3+}, which is attributed to implantation induced disorder rather than Gd^{3+} related transitions, and the emission intensity decreases with increase of Gd^{3+} doping. Broad violet emission band around 3.15 eV due to RE implantation in ZnO was reported, which is assigned to the vacancy related emission [9]. Doping of Gd^{3+} in ZnO exhibits radiative transition around 318 nm due to transition between the first excited $^6P_{7/2}$ state and the $^8S_{7/2}$ ground state, which is similar to the cathode-luminescence spectra in Gd doped GaN [10].

In addition to the photoluminescence (PL) studies, numerous works have been reported on the magnetic behavior of transition metal doped semiconductors [11,12]. A theoretical prediction by Dietl *et al*. [13] demonstrated that the Curie temperature can be increased above room temperature in p-type semiconductor based diluted magnetic semiconductors (DMS). In fact, first-principles calculations show that the ferromagnetic state of GaN is stable for various doping elements, including V, Cr, or Mn, without any additional carrier doping [14,15]. In rare earth elements, the 4f electrons are localized, exchange interactions are possible via 5d or 6s conduction electrons, but the high orbital momentum leads to high total magnetic moments (e.g., 8 µB per Gd atom). Dhar *et al*. [16] have studied room temperature ferromagnetism (RT-FM) coupling in Gd doped GaN with a magnetic moment of 4000 µB per Gd atom, which is very high when compared to its intrinsic atomic moment of 8 µB per Gd atom. This motivates us to study the luminescence and magnetic properties of Gd^{3+} doped ZnO. We found that the photoluminescence of Gd^{3+} doped ZnO shows an obvious intense violet–blue emission and paramagnetic behavior at room temperature.

2   Experimental procedure

Solid-state reaction was employed for the preparation of $Zn_{1-x}Gd_xO$ ($x = 0$, 0.02, 0.04, 0.06, and 0.08) ceramic samples. The starting reagents used included high purity ZnO (99.9%, Sigma Aldrich) and Gd_2O_3 (99.9%, Sigma Aldrich). The stoichiometric amounts of starting materials were ball milled for 30 h and the resultant powders were calcined at 1000 ℃ for 7 h under ambient conditions. The heating and cooling

rates were maintained at 10 ℃/min. The powder X-ray diffraction (XRD) patterns were recorded on Phillips X'PERT PRO diffractometer with Cu Kα radiation. The morphology of as synthesized powders was studied using transmission electron microscopy (TEM), recorded in JEOL-TEM 2010 with an accelerating voltage of 200 kV. The optical absorption measurements were performed using JASCO-V-670 spectrophotometer. The room temperature photoluminescence spectra were recorded on a PTI (Photon Technology International) fluorimeter with an Xe arc lamp of 60 W power. The magnetic measurements were carried out using a superconducting quantum interference device (SQUID, Quantum Design MPMS-XL7).

3   Results and discussion

Figure 1 shows the powder XRD patterns of $Zn_{1-x}Gd_xO$ ($x = 0$, 0.02, 0.04, 0.06, and 0.08) ceramics calcined at 1000 ℃ for 7 h. In the case of Gd doped ZnO, the XRD patterns reveal the presence of single phase wurtzite structure (JCPDS Card No. 36-1451) with a space group of $P6_3mc$. Surprisingly, no diffraction peaks of Gd_2O_3 are observed in these XRD patterns implying the incorporation of Gd^{3+} into the dopant site. The Gd^{3+} ions are successfully incorporated into ZnO ceramics, and the peaks are broadened with increasing Gd^{3+} content. The relative peak intensity of diffraction peaks decreases with the increasing Gd^{3+} content. This decrease can be attributed to the decreasing crystallinity due to reduction of crystallite size and/or the difference in the ionic radius of Gd^{3+} (0.93 Å) and
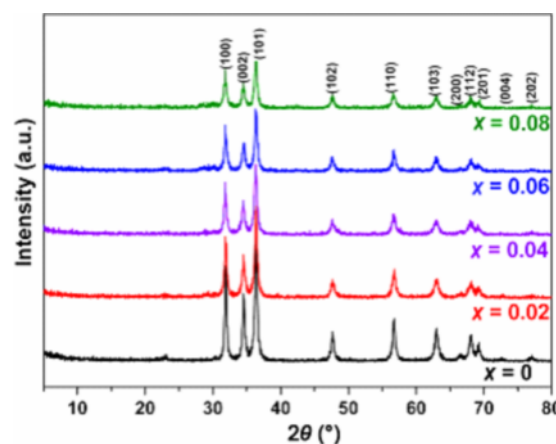
Fig. 1   XRD patterns of $Zn_{1-x}Gd_xO$ ($x = 0$, 0.02, 0.04, 0.06, and 0.08) nano-ceramics.

Zn^{2+} (0.74 Å). A marginal systematic variation in the peak positions of (100), (002), and (101) planes to lower angles is observed due to the substitution of diluted quantity of the Gd^{3+} ions. However, a slight anomaly in the peak position of the (101) plane for $x =$ 0.02 to higher angle may be attributed to the internal compressive micro stress due to the substitution of Gd^{3+} [17]. The crystallite sizes of all the synthesized samples were calculated from diffraction peak broadening using Scherrer's equation:

$$D = \frac{0.94\lambda}{\beta \cos\theta} \quad (1)$$

where D is the average crystallite size, β is the full width half maximum (FWHM) of XRD peak in radian, θ is the position of the diffraction peak, and λ (1.5418 Å) is the wavelength of X-ray radiation used. The evaluated crystallite sizes of all the samples are shown in Table 1. The crystallite size reduces reasonably with increasing Gd^{3+} content. The morphology of as synthesized ZnO and $Zn_{1-x}Gd_xO$ ($x = 0.04$) ceramic powders are shown in Figs. 2(a) and 2(b), respectively. It can be seen that most of the particles are in a narrow size range except for few particles with an irregular shape and agglomeration. The agglomerates observed might be due to the calcination process. In the TEM analysis using dispersed powders, the particles show nano-sized nearly spherical morphology, with an average size of 60 nm. The selected area electron diffraction (SAED) pattern showing concentric rings implies polycrystalline nature of the nano-ceramic powders as shown in the inset of Fig. 2(b). All the observed diffraction rings could be attributed to the ZnO wurtzite structure consistent with the XRD patterns shown in Fig. 1.

The absorption of a photon, leading to excitation of an electron from the valence band to the conduction band, is associated with the band gap energy. The optical absorption spectra of ZnO and Gd^{3+} doped ZnO ceramic samples are shown in Fig. 3. It can be seen that with the increase in Gd^{3+} dopant concentration, the

Table 1 Average crystallite size, band gap energy, and magnetic moment of $Zn_{1-x}Gd_xO$ ($x = 0$, 0.02, 0.04, 0.06, and 0.08) samples

Composition x	Crystallite size (nm)	Band gap energy (eV)	Magnetic moment (emu/g)
0	54	3.42	—
0.02	53	3.25	0.0791
0.04	46	3.14	0.1758
0.06	44	3.12	0.8290
0.08	41	3.05	1.4568
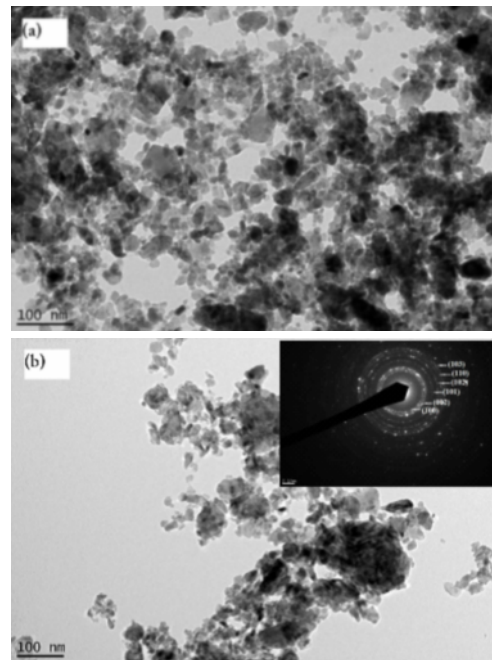
Fig. 2 TEM micrographs of (a) pure ZnO and (b) $Zn_{1-x}Gd_xO$ ($x = 0.04$) nano-ceramics with the inset showing the corresponding SAED pattern.
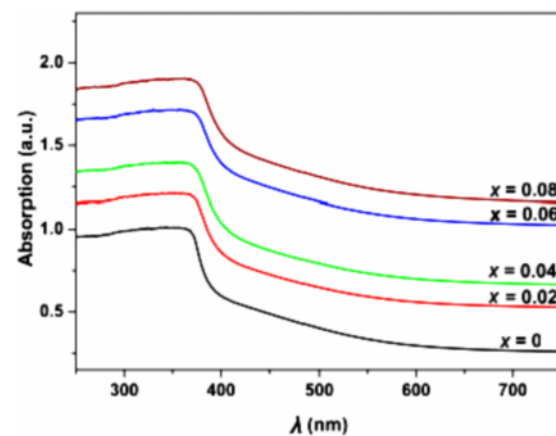
Fig. 3 Optical absorption spectra of $Zn_{1-x}Gd_xO$ ($x = 0$, 0.02, 0.04, 0.06, and 0.08) samples.

peaks shift towards higher wavelength region.

The relation between the absorption coefficient and the incident photon energy can be calculated by the following equation [18]:

$$\alpha h\nu = A(h\nu - E_g)^{1/2} \quad (2)$$

where α is the absorption coefficient, $h\nu$ is the photon energy, A is a constant, and E_g is the optical direct band gap. It is known that the optical band gap of the $Zn_{1-x}Gd_xO$ ceramic samples has a direct optical transition. The corresponding direct band gaps of the pure ZnO and doped samples have been evaluated by

fitting and extrapolating the linear portion of $(\alpha h\nu)^2$ vs. $(h\nu)$ plot to $\alpha = 0$ as shown in Fig. 4. The band gap energy (E_g) values are given in Table 1. Liu *et al.* [19] have observed blue shift in Gd doped ZnO quantum dots with reducing size of particles. In our case, it is seen that E_g values decrease with increasing Gd content. In general, the band gap of nanoparticles blue-shifts with decrease in size; however, here, despite a reasonable decrease in size, the band gap is red shifting (Table 1). This is possibly due to the systematic inclusion of the Gd impurities in the ZnO structure inducing the formation of new recombination centers lowering the band gap energy. In addition, this red shift of gap energy may also be due to the increase in carrier concentration with Gd^{3+} doping.

Photoluminescence is a sensitive non-destructive technique to investigate the intrinsic and extrinsic defects in semiconductors. The room temperature PL emission spectra of pure ZnO and Gd doped ZnO samples are shown in Fig. 5 with an excitation wavelength of 325 nm from Xe lamp source. All samples exhibit a multimode superimposed broad emission bands with peak at 420 nm and a weak band at 550 nm. The multimode peak is de-convoluted and found to have four peaks centered around 398, 420, 445, and 468 nm. The wavelength range of the broad multimode peak spans the violet and blue regions of the visible spectrum leading to a dominant bi-chromic visible emission. Similar kind of broad violent–blue emission extending from violet to blue with a distinct peak at 420 nm was reported in rare earth implanted ZnO samples [9]. The 420 nm peak corresponds to the near band-edge (NBE) emission of ZnO. The NBE
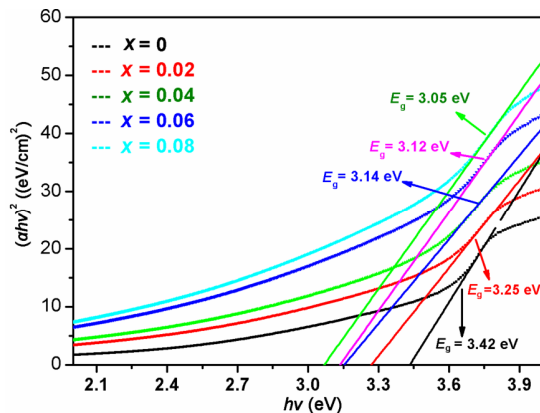
Fig. 4 $(\alpha h\nu)^2$ vs. $(h\nu)$ plots for $Zn_{1-x}Gd_xO$ ($x = 0$, 0.02, 0.04, 0.06, and 0.08) samples.

emission is attributed to the radiative recombination of a hole in the valence band and an electron in the conduction band [20]. The strong PL emission at 420 nm is well corroborated with the previous report on ZnO quantum dots [21]. The origin of the visible luminescence from ZnO is greatly controversial, especially for the violet–blue emission around 400 nm. The Zn vacancies and surface defects are the main structural defects that occur in ZnO semiconductor during their preparation. It is believed that they generate trapping centers in the band gap leading to luminescence in the visible wavelength region. Recently, Zeng *et al.* [22] reported that the violet–blue emission can be interpreted by the transition of extended zinc interstitials (Zn_i) states lying below the conduction band minima. Here, we observe a broad and strong violet–blue emission band even in pure ZnO due to radiative recombination. The broadening of violet–blue emission peak could be attributed to hybridization of various defect states induced by the non-equilibrium ball milling method of preparation and size distribution. In addition, a much weaker peak is located at 550 nm which is attributed to the surface defects from oxygen vacancies or Zn_i [23]. Vanheusden *et al.* [24] found that oxygen vacancies are responsible for the green luminescence in ZnO. Oxygen vacancies occur in three different charge states: the neutral oxygen vacancy (V_O^0), the singly ionized oxygen vacancy (V_O^*), and the doubly ionized oxygen vacancy (V_O^{**}) of which only V_O^* can act as the so called luminescent center [25].
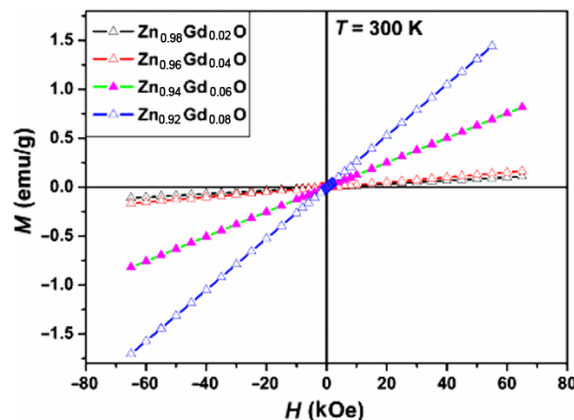
In the present study, the PL intensity increases with Gd doping and reaches a maximum for the critical concentration of 4 mol% of Gd. Beyond the critical concentration, the emission intensity gradually decreases (Fig. 5). Similar emission quenching has been reported in alkali doped ZnO nanorods [26]. The optical transition that is responsible for Gd^{3+} emission is $^6P_J \rightarrow {}^8S_{7/2}$ (4f–4f transition), so the incorporation of Gd^{3+} could improve the emission intensity of rare earth ions. Murmu *et al.* [27] have also observed this for green emission with red shifting of emission peak of Gd doped ZnO single crystals measured at low temperature. Moreover, trivalent Gd^{3+} ions act as a charge compensator to enter the surrounding of Zn^{2+} ions. In this case, excess doping perhaps causes quenching of luminescence. Lopez *et al.* [28] reported that the oxygen vacancies might be sensitizers for the
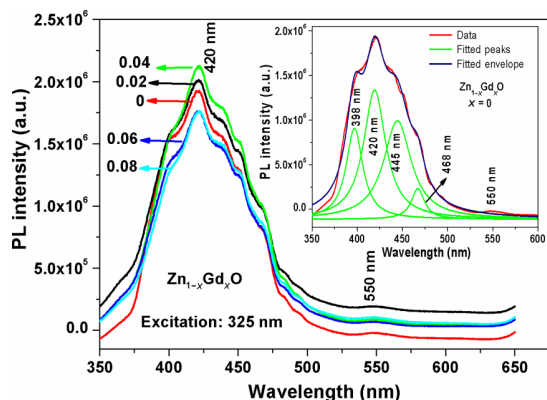
Fig. 5 Photoluminescence emission spectra of $Zn_{1-x}Gd_xO$ ($x = 0$, 0.02, 0.04, 0.06, and 0.08) samples. Inset is the representative de-convoluted multimodal peaks for pure ZnO.

Fig. 6 Magnetization (*M*) as a function of applied magnetic field (*H*) of $Zn_{1-x}Gd_xO$ ($x = 0.02$, 0.04, 0.06, and 0.08) samples at 300 K.

energy transfer to the rare earth ion due to the strong mixing of charge transfer states, resulting in highly enhanced luminescence. However, excess oxygen vacancies in the host would inevitably destroy the crystallinity, which leads to quenching of the luminescence. Therefore, we firmly believe that the characteristic strong violet–blue emission in ZnO ceramics results from the band edge emission and the associated defects by virtue of doping and high energy ball milling. With conventional growth methods, to obtain a prominent emission, the as-grown ZnO usually requires some additional treatment, such as surface modification and annealing. The varying violet–blue emission intensities confirm that the Gd^{3+} ions are successfully incorporated into the ZnO ceramics.

Figure 6 shows the *M* vs. *H* magnetization measurements carried out at 300 K for the $Zn_{1-x}Gd_xO$ ($x = 0.02$, 0.04, 0.06, and 0.08) nano-ceramic powder samples. Pure ZnO displays diamagnetic behavior (not shown here). The curves show no hysteresis at room temperature for the studied samples. From the XRD and TEM results, no impurity phases are detected, so spurious ferromagnetic like signal is ruled out. Recently, Dakhel *et al.* [17] reported ferromagnetism in Gd doped ZnO nanocrystalline powders prepared by co-precipitation technique. There are reports on ferromagnetism (FM) and antiferromagnetism in Gd doped ZnO. In our case, typical feature of paramagnetic behavior have been observed for all Gd^{3+} concentrations. Paramagnetism is expected to arise from the exchange interaction of magnetic moments mediated by the defects in doped nanoceramics. Similar paramagnetic behavior was reported for

transition metal doped ZnO and SnO_2 [29–33]. Adhikari *et al.* [34] observed the absence of ferromagnetic and antiferromagnetic ordering in Gd doped SnO_2 nanoparticles. They also identified that with increasing Gd content, size of the particles decreases and due to which the surface spin effects lead to enhanced Gd–O–Gd interactions. The magnetic moment (*M*) of the gadolinium doped samples increasing linearly with increasing Gd^{3+} content is given in Table 1, which demonstrates substitution of Gd^{3+} ions replacing the Zn^{2+} sites in the wurtzite lattice. The values of magnetic moment are much less than the actual moment of 8 μB per Gd atom. The observed paramagnetic behavior might be due to random distribution of the Gd^{3+} ions in ZnO giving rise to formation of some sort of weak interaction depending on composition and distance between the magnetic dopants, thereby influencing the strength of direct or indirect coupling among the magnetic ions. Our observation of paramagnetism in Gd doped ZnO is well supported by the recent theoretical report using density functional theory which predicts "paramagnetic" ground state for wurtzite ZnO lattice at room temperature based on the distance between the magnetic ions [35].

4 Conclusions

Single phase nanocrystalline Gd^{3+} doped ZnO ceramics was successfully synthesized by solid-state reaction. The morphology of the as prepared samples were nearly spherical in shape with an average diameter of 60 nm from the TEM results. Red shift in band gap

observed with increasing Gd^{3+} was attributed to the increase in carrier concentration by Gd^{3+} doping. Strong bi-chromic violet–blue visible emission was observed, and the emission intensity increased with Gd^{3+} doping until it reached a critical concentration of 4 mol% of Gd^{3+}. The magnetic measurements of Gd doped ZnO exhibited paramagnetism at room temperature.

Acknowledgements

References

[1] Kang HS, Ahn BD, Kim JH, *et al*. Structural, electrical, and optical properties of *p*-type ZnO thin films with Ag dopant. *Appl Phys Lett* 2006, **88**: 202108.

[2] Huang GJ, Wang JB, Zhang XL, *et al*. Synthesis, structure, and room-temperature ferromagnetism of Ni-doped ZnO nanoparticles. *J Mater Sci* 2007, **42**: 6464–6468.

[3] Hng H-H, Knowles KM. Microstructure and current–voltage characteristics of multicomponent vanadium doped zinc oxide varistors. *J Am Ceram Soc* 2000, **83**: 2455–2462.

[4] Phan T-L, Vincent R, Cherns D, *et al*. Electron spin resonance and Raman studies of Mn-doped ZnO ceramics. *J Appl Phys* 2007, **101**: 09H103.

[5] Li H, Qin X, Zhang W, *et al*. Synthesis of Co-doped ZnO nanofibers and their magnetic properties. *J Am Ceram Soc* 2012, **95**: 217–222.

[6] Song H, Kim YJ. Characterization of luminescent properties of ZnO:Er thin films prepared by rf magnetron sputtering. *J Eur Ceram Soc* 2007, **27**: 3745–3748.

[7] Pillai SK, Sikhwivhilu LM, Hillie TK. Synthesis, characterization and photoluminescence properties of Dy^{3+}-doped nano-crystalline SnO_2. *Mater Chem Phys* 2010, **120**: 619–624.

[8] Ney V, Ye S, Kammermeier T, *et al*. Structural, magnetic, and optical properties of Co- and Gd-implanted ZnO(0001) substrates. *J Appl Phys* 2008, **104**: 083904.

[9] Monteiro T, Neves AJ, Carmo MC, *et al*. Optical and structural analysis of bulk ZnO samples udoped and rare earth doped by ion implantation. *Superlattice Microst* 2006, **39**: 202–210.

[10] Choi SW, Emura S, Kimura S, *et al*. Emission spectra from AlN and GaN doped with rare earth elements. *J Alloys Compd* 2006, **408–412**: 717–720.

[11] Sharma P, Gupta A, Rao KV, *et al*. Ferromagnetism above room temperature in bulk and transparent thin films of Mn-doped ZnO. *Nat Mater* 2003, **2**: 673–677.

[12] Wei X, Skomski R, Balamurugan B, *et al*. Magnetism of TiO and TiO_2 nanoclusters. *J Appl Phys* 2009, **105**: 07C517.

[13] Dietl T, Ohno H, Matsukura F, *et al*. Zener model description of ferromagnetism in zinc-blende magnetic semiconductors. *Science* 2000, **287**: 1019–1022.

[14] Sato K, Katayama-Yoshida H. Material design of GaN-based ferromagnetic diluted magnetic semiconductors. *Jpn J Appl Phys* 2001, **40**: L485–L487.

[15] Akinaga H, Manago T, Shirai M. Material design of half-metallic zinc-blende CrAs and the synthesis by molecular-beam epitaxy. *Jpn J Appl Phys* 2000, **39**: L1118–L1120.

[16] Dhar S, Brandt O, Ramsteiner M, *et al*. Colossal magnetic moment of Gd in GaN. *Phys Rev Lett* 2005, **94**: 037205.

[17] Dakhel AA, El-Hilo M. Ferromagnetic nanocrystalline Gd-doped ZnO powder synthesized by coprecipitation. *J Appl Phys* 2010, **107**: 123905.

[18] Tauc J. *Amorphous and Liquid Semiconductor*. New York: Plenum Press, 1974.

[19] Liu Y, Ai K, Yuan Q, *et al*. Fluorescence-enhanced gadolinium-doped zinc oxide quantum dots for magnetic resonance and fluorescence imaging. *Biomaterials* 2011, **32**: 1185–1192.

[20] Jin BJ, Im S, Lee SY. Violet and UV luminescence emitted from ZnO thin films grown on sapphire by pulsed laser deposition. *Thin Solid Films* 2000, **366**: 107–110.

[21] Fu YS, Du XW, Kulinich SA, *et al*. Stable aqueous dispersion of ZnO quantum dots with strong blue emission via simple solution route. *J Am Chem Soc* 2007, **129**: 16029–16033.

[22] Zeng H, Duan G, Li Y, *et al*. Blue luminescence of ZnO nanoparticles based on non-equilibrium process: Defect origins and emission controls. *Adv Funct Mater* 2010, **20**: 561–572.

[23] Kang HS, Kang JS, Kim JW, *et al*. Annealing effect on the property of ultraviolet and green emissions of ZnO thin films. *J Appl Phys* 2004, **95**: 1246–1250.

[24] Vanheusden K, Warren WL, Seager CH, *et al*. Mechanism behind green photoluminescence in ZnO phosphor powders. *J Appl Phys* 1996, **79**: 7983–7990.

[25] Li W, Mao D, Zhang F, *et al*. Characteristics of ZnO:Zn phosphor thin films by post-deposition annealing. *Nucl Instrum Meth B* 2000, **169**: 59–63.

[26] Chawla S, Jayanthi K, Kotnala RK. Room-temperature ferromagnetism in Li-doped *p*-type luminescent ZnO nanorods. *Phys Rev B* 2009, **79**: 125204.

[27] Murmu PP, Mendelsberg RJ, Kennedy J, *et al*. Structural and photoluminescence properties of Gd implanted ZnO single crystals. *J Appl Phys* 2011, **110**: 033534.

[28] Lopez OA, Mckittrick J, Shea LE. Fluorescence properties of polycrystalline Tm^{3+}-activated $Y_3Al_5O_{12}$ and Tm^{3+}–Li^+ co-activated $Y_3Al_5O_{12}$ in the visible and near IR ranges. *J Lumin* 1997, **71**: 1–11.

[29] Yin S, Xu MX, Yang L, *et al*. Absence of ferromagnetism in bulk polycrystalline $Zn_{0.9}Co_{0.1}O$. *Phys Rev B* 2006, **73**: 224408.

[30] Wang W, Wang Z, Hong Y, *et al*. Structure and magnetic properties of Cr/Fe-doped SnO_2 thin films. *J Appl Phys* 2006, **99**: 08M115.

[31] Sambasivam S, Choi BC, Lin JG. Intrinsic magnetism in Fe doped SnO_2 nanoparticles. *J Solid State Chem* 2011, **184**: 199–203.

[32] Qi J, Gao D, Liu J, *et al*. Magnetic properties of Er-doped ZnO films prepared by reactive magnetron sputtering. *Appl Phys A* 2010, **100**: 79–82.

[33] Sambasivam S, Joseph DP, Jeong JH, *et al*. Antiferromagnetic interactions in Er-doped SnO_2 DMS nanoparticles. *J Nanopart Res* 2011, **13**: 4623–4630.

[34] Adhikari R, Das AK, Karmakar D, *et al*. Gd-doped SnO_2 nanoparticles: Structure and magnetism. *J Magn Magn Mater* 2010, **322**: 3631–3637.

[35] Bantounas I, Singaravelu V, Roqan IS, *et al*. Structural and magnetic properties of Gd-doped ZnO. *J Mater Chem C* 2014, **2**: 10331–10336.